Supersonic Retro-Propulsion for Future High-Mass Robotic Mars Lander Missions

By Marcus LOBBIA,[1] Aron WOLF,[1] and Charles WHETSEL[1]

[1]*NASA Jet Propulsion Laboratory, California Institute of Technology, USA*

(Received June 21st, 2017)

A feasibility study was conducted to investigate the potential performance advantages of Supersonic Retro-Propulsion in support of future high-mass Mars robotic landing missions. A notional reference architecture for a potential future Mars Sample Return formed the basis for assuming a 4.7 m diameter SRP entry vehicle containing the Mars Ascent Vehicle element. Configuration analysis was conducted to ensure that the payload and required SRP components (including engines and propellant) fit within in the capsule volume. Optimized trajectory analysis highlighted several key performance sensitivities of SRP for ballistic coefficients of 150, 300, and 450 kg/m2. These results indicated a broad SRP ignition envelope (1-4 km altitude, 300-750 m/s velocity), as well as relatively small propellant mass fraction sensitivities to SRP thrust/weight, landing site elevation, and the application of a 4-g entry deceleration constraint (relevant for future crewed mission trajectories). Finally, mass-sizing was performed to assess sensitivities to ballistic coefficient and entry velocity, and showcased the ability of the SRP system to land payload masses on the order of twice that of MSL.

Key Words: Mars, Entry, Supersonic Retro-Propulsion

Nomenclature

BC	:	ballistic coefficient
C_3	:	characteristic energy
g	:	Earth gravity
Isp	:	specific impulse
L_S	:	Mars solar latitude
q	:	dynamic pressure
T	:	thrust
W	:	weight

1. Introduction

The 2012 Mars Science Laboratory (MSL) Entry, Descent, and Landing (EDL) was successful in depositing on the surface of Mars the largest payload (by a large measure) landed to date. To achieve this, new technologies for Mars EDL, such as a guided lifting entry, skycrane maneuver, and more were required.[1] For future missions to be able to land even heavier payloads on Mars, the continued use of supersonic parachutes will require an extensive test and development program to qualify new designs at larger diameters than have ever been tested/flown before. As an alternative, the Jet Propulsion Laboratory (JPL) and other organizations have been investigating the use of supersonic retro-propulsion (SRP) to eliminate the need for supersonic parachutes. Additional benefits of this approach include potentially enhanced landing accuracy, and combining the SRP propulsion system with aspects of the final descent landing propulsion to simplify the overall design.

While not a new technology, SRP has gained traction in recent years with Space-X's demonstrations during booster flyback of its Falcon 9 rocket, and announcement that it plans to land a "Red Dragon" vehicle on Mars in the near future using SRP.[2] JPL has also looked at SRP to support landing high-mass components of a potential Mars Sample Return (MSR) mission,[3] and as a candidate architectural component for human Mars missions.[4]

The present work provides details of the development of a high-ballistic coefficient SRP concept at JPL to support MSR-class payloads. The concept implements bi-propellant propulsion, and trades are conducted to assess the effects of Thrust/Weight (T/W) and other parameters on landing system performance. A mass-sizing model is presented, and considerations related to configuration and packaging of required components are discussed.

2. Mars Sample Return Architecture

The most recent planetary science decadal survey indicated that the Mars Astrobiology Explorer-Cacher element of a potential robotic MSR campaign should be considered as the highest-priority large-class mission.[4] While there is currently no specific plan or schedule for MSR, NASA is engaged in a variety of related technology and risk reduction activities.[5-6] Future Mars mission concepts are also being studied that could perform elements of a future sample return, starting with the sample caching function of the upcoming Mars 2020 mission.

The current approach is based on a notional MSR reference architecture consisting of three separately-launched elements, as shown in Fig. 1: 1) a sample-caching rover (such as Mars 2020), 2) a Mars orbiter containing on-orbit Orbiting Sample (OS) capture equipment and an Earth Entry Vehicle (EEV), and 3) a Mars Ascent Vehicle (MAV), OS container, and a mobile MAV rover platform. For the third element, studies are also being done to trade the pros/cons of a fetch rover concept (where a small rover will retrieve the samples and bring them

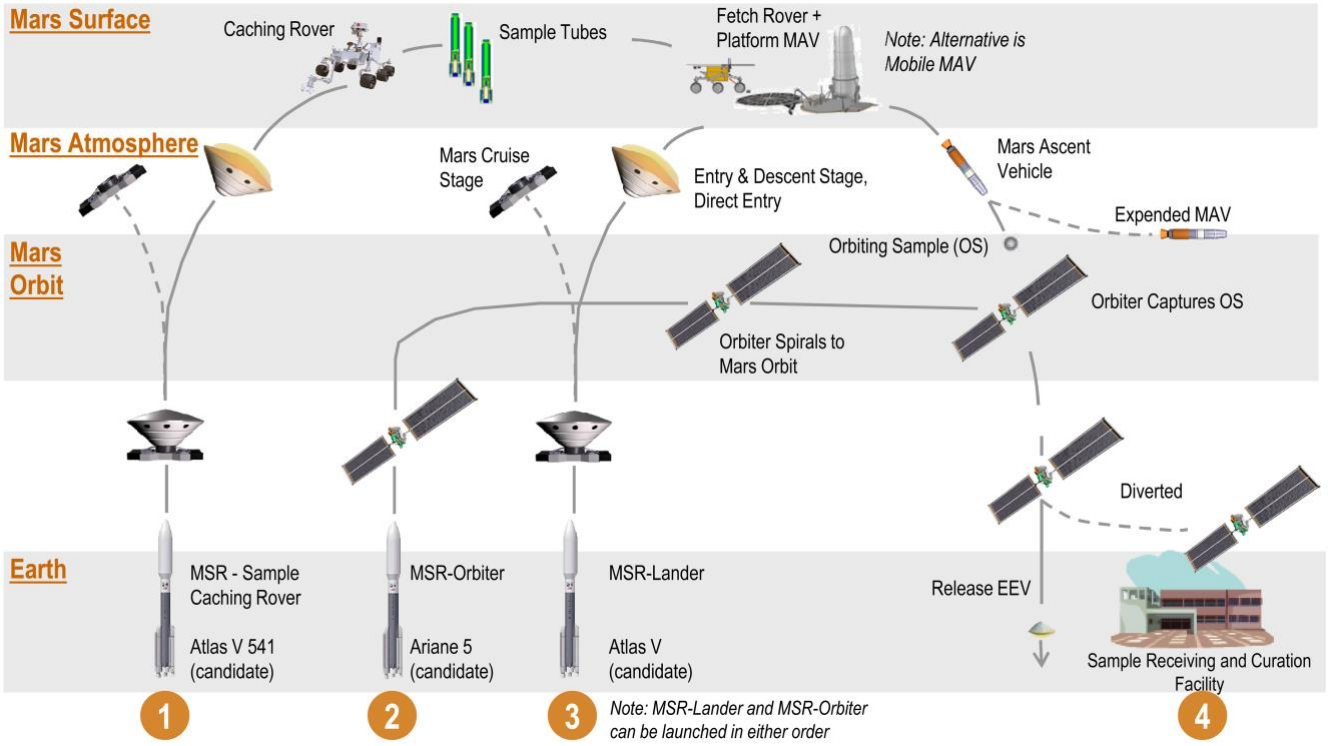

Fig. 1. Notional Mars Sample Return architecture, consisting of four primary elements.

back to a stationary MAV) against a mobile MAV concept. Finally, the fourth element of the architecture is the Sample Receiving and Curation Facility located on Earth, to provide a safe environment for sample analysis and storage.

The work described in this paper focuses on performance trades involving SRP for the "MSR-Lander" MAV/OS element shown in Fig. 1. The candidate launch vehicle (LV) for the MSR-Lander is an Atlas V, which would imply the use of a MSL-derived descent stage. While this may be feasible, current expectations are that the landed mass requirement will increase over MSL and Mars 2020. This could require a newer/larger supersonic parachute that will need to go through extensive design activities and qualification tests, or could potentially require a much larger diameter aeroshell to maintain feasible supersonic parachute deployment conditions. As an alternative, the present work is focused on assessing the viability of a high-ballistic coefficient SRP-based descent stage for this MSR-Lander element.

3. Supersonic Retro-Propulsion Concept

3.1. Launch Vehicle Assumptions

One of the primary considerations driving the SRP configuration is the LV performance and fairing size. As the candidate MSR architecture shown in Fig. 1 indicates an Atlas V as the possible choice for the MSR-Lander, the assumption of a 5 m diameter LV fairing is enforced, resulting in a maximum possible MSR-Lander aeroshell diameter of 4.7 m. However, as multiple LVs are in development and planned for operation by the time an MSR-Lander would be launched, additional LVs (see Table 1) with higher launch mass capabilities were also considered.

Table 1. Launch vehicle performance capability[8] to Mars

	2026 Opportunity C_3=9.14 km^2/s^2	2028 Opportunity C_3=8.93 km^2/s^2
Falcon Heavy	10075 kg	10130 kg
Delta IV Heavy	8600 kg	8635 kg
Atlas V 551	5150 kg	5170 kg

3.2. Aeroshell

All NASA Mars landers have used a 70 deg. sphere-cone shape, which draws heritage from the Mars Viking Landers. While this shape provides suitable drag for a Mars entry mission, a spherical aeroshell can potentially provide more volume for packaging of a large MSR-Lander configuration. A spherical aeroshell can also provide the benefit of lower heating (and a corresponding reduction in TPS mass). Studies have shown that the eliminating the discontinuity in curvature between the nose cap and cone frustum results in a favorable pressure gradient over the entire lee-side (when flown at angle of attack similar to MSL), and avoids increased turbulent heating due to the sonic line attachment at the cap/cone junction.[9]

Based on data on similar spherical aeroshell capsule shapes, a series of ballistic coefficients were selected for analysis in the current study (see Table 2). The corresponding entry mass at Mars (based on a nominal hypersonic drag coefficient of 1.46) is also shown. While the largest ballistic coefficient (450 kg/m^2) case results in an entry mass exceeding the launch capabilities shown in Table 1, it is still assessed due to the current development status and potential for performance increase for the Falcon Heavy and other future LVs.

Table 2. Ballistic coefficients and corresponding entry masses at Mars

Ballistic Coeff., kg/m2	150	300	450
Entry Mass, kg	3813	7627	11440

3.3. Propulsion System

SRP places a relatively large emphasis on the propulsion system to decelerate the entry capsule from supersonic Mach numbers, as well as to support the final descent. For this purpose, electrically pumped Nitrogen-Tetroxide /Monomethyl-hydrazine (NTO/MMH) bi-prop engines are assumed. A nozzle area expansion ratio of 24:1 is implemented based on maintaining a high *Isp* (295 s) while meeting aeroshell accommodation constraints.

A modular system with multiple engines provides scalability to meet *T/W* requirements for different ballistic coefficient cases. Engine full-thrust ratings of 8000 N and 12000 N are assumed for the 300 kg/m2 and 450 kg/m2 ballistic coefficient cases, respectively. For a *T/W*=3, this results in 12 engines, whereas 20 engines are required for the *T/W*=5 scenarios. Turning off individual engines and an assumed per-engine throttle-capability (65%) allows the system to meet the range of thrust requirements from initial SRP deceleration to final descent and landing.

As previously mentioned, the configurations considered in this study, the engines are electrically-pump driven. Recent advances in Lithium-Ion battery technology, coupled with the relatively short required run time of approximately one minute, make this a less complex alternative to turbo-pumps. The present work relies on an assumed battery energy density of 150 W-hr/kg, although this is projected to rise to 300-400 W-hr/kg by the potential timeframe of an MSR mission.

3.4. Configuration

Initially both a landed configuration (i.e., landing with the heatshield attached on integrated landing legs) and a "skycrane" based configuration (similar to that used on MSL[1]) were investigated (see Fig. 2). Subsequent analysis later focused on the landed configuration, as this provides better packaging characteristics with the propellant tanks located below the rover payload deck, and the complexity of jettisoning the heatshield with integrated SRP engines is avoided. The remainder of the analysis and results of the present work focus on the landed configuration, although alternative variants of the skycrane configuration (e.g., with different sets of engines integrated into the heatshield and backshell to facilitate heatshield separation) will be studied in future iterations of this work.

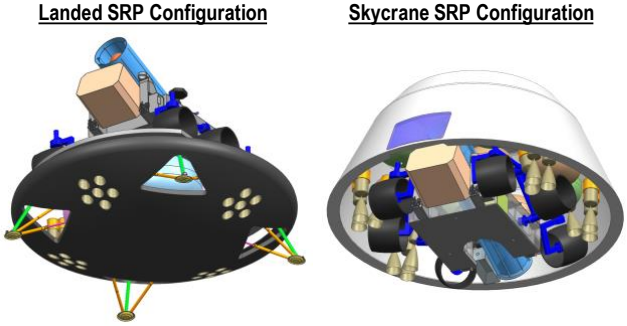

Fig. 2. Potential SRP configuration options – baseline assumes Landed Configuration (left).

For the landed SRP configuration, a set of four landing legs provide final landing support. For the Mobile MAV concept, Rover egress could be enabled via either jettison of the backshell prior to landing (with fold-out ramps), or by deploying the backshell on landing to form an integrated ramp (see Fig. 3). These concepts provide notional feasibility of the egress approach, but were not assessed in detail as they did not influence the system performance parameters examined in this study. Detailed study of the landing and egress system is planned in future design/analysis efforts.

3.5. Trajectory, Guidance, and Control

To assess the performance sensitivity to various SRP system parameters, a nominal trajectory model was developed,[10-11] with the key inputs of: entry velocity, entry flight path angle (EFPA), ballistic coefficient, and use of a deceleration load constraint (to provide a path for demonstrating *g*-limited SRP entries as a human mission precursor). The trajectory model optimizes EFPA, bank profile, SRP ignition time, and thrust profile, with the objective of minimizing propellant mass fraction (PMF) of the entry system. For the purposes of this work, PMF is defined as (propellant mass at ignition) / (total wet mass at ignition). Constraints include a minimum bank angle of 25 deg. and a lofting constraint with a flight path angle ≤1 deg. The trajectory ends with a required descent rate of 0.75 m/s at a -90 deg. flight path angle, and propellant is allocated to enable

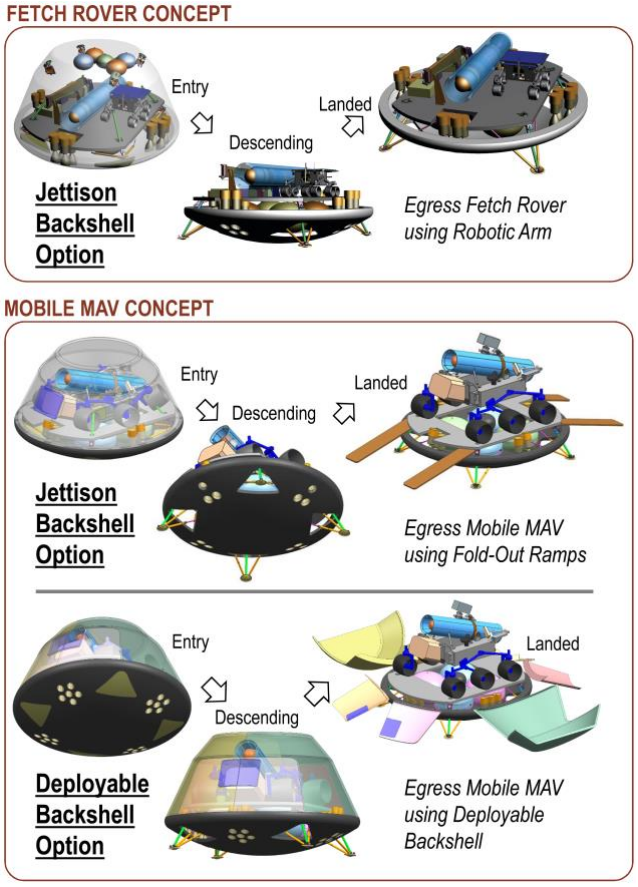

Fig. 3. Possible SRP rover egress options for landed configuration.

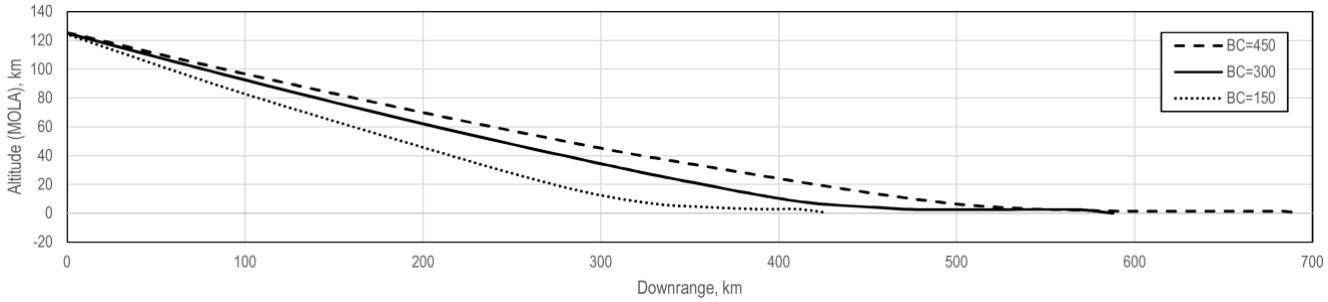

Fig. 4. Altitude vs. downrange shown for different ballistic coefficient trajectories, up until SRP ignition point.

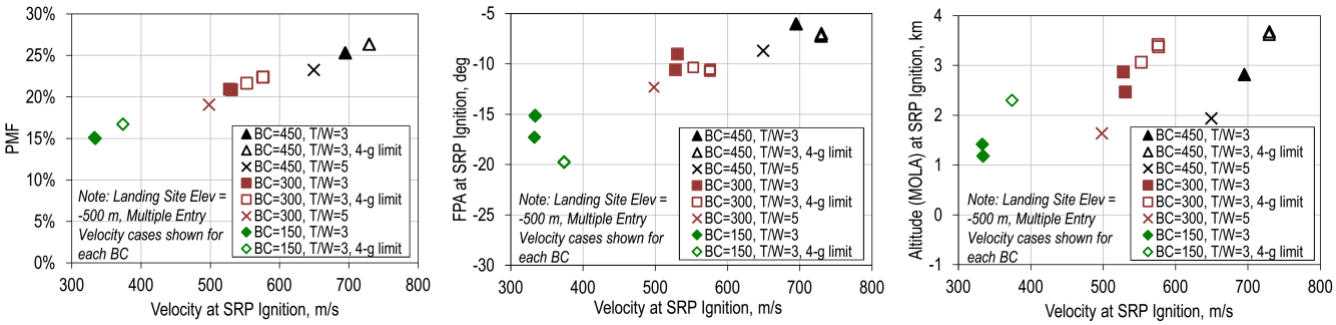

Fig. 5. Trajectory performance sensitivity to SRP ignition velocity.

Table 3. Parametric study inputs assessed.

Ballistic Coefficient (BC), kg/m2	150, 300, 450
T/W	3, 5
Landing Site Elevation (MOLA1), km	-0.5, -1.5, -2.5, -3.5
Entry Velocity, km/s	4.5, 5.5, 6.5, 7.5

1*Mars Orbiter Laser Altimeter*

a powered hover for 20 sec.

3.6. Mass Estimation

One of the key figures of merit in assessing the SRP system performance is to provide an estimate of the landed mass capable for a given entry ballistic coefficient. For this purpose, a moderate-fidelity mass sizing model was developed using a combination of physics-based sizing methods and historical sizing relationships developed from previous Mars entry missions (e.g., MSL, Mars Exploration Rover, Mars Pathfinder, and Phoenix).[12] Key inputs include the ballistic coefficient, geometry, and desired propellant mass fraction. The model uses an iterative sizing technique to account for inter-subsystem dependencies, and provides a detailed mass breakout at the subsystem and component levels.

Currently the Aeroshell thermal protection system (TPS) mass is estimated by scaling a notional reference Phenolic-Impregnated Carbon Ablator (PICA) TPS concept to meet the required TPS mass fraction (based on the trajectory aeroheating and a TPS sizing relationship[13]). Plans are in place to improve this in future design exercises using a transient thermal/ablation-response analysis, as well as to perform a more rigorous assessment of the TPS material suitability for the expected aerothermal environments.

4. Results

To investigate the feasibility and suitability of SRP for a future MSR-Lander mission, a parametric analysis was conducted to assess the performance sensitivity to a variety of inputs (see Table 3). An assumed worst-case atmosphere model was used based on a Mars solar longitude (L_S) of approximately 150 deg.

As discussed above, the trajectory analysis assumed a hypersonic drag coefficient of 1.46 until SRP ignition. Once SRP was initiated, however, the aerodynamic drag was set to zero to provide a conservative set of results, as the SRP flowfield is complex and previous studies have indicated that drag may be reduced substantially depending on the location, number, and thrust coefficient of the engines.[14]

A comparison of nominal optimized trajectories for the three different ballistic coefficient cases is shown in Fig. 4. It can be observed that, in order to minimize PMF, the larger ballistic coefficient cases tend to fly longer downrange, and SRP ignition occurs at a shallower FPA. This is likely due to the larger kinetic energies, and the trajectory optimizer's attempt to dissipate this to the extent possible prior to SRP ignition.

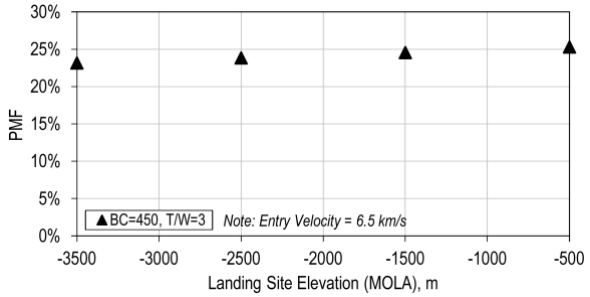

Fig. 6. PMF vs. Landing Site Elevation trend.

Figure 5 shows some of the key sensitivity results with respect to SRP ignition velocity, and several trends are visible in the results. For example, as expected a higher SRP ignition velocity results in a higher PMF, and an approximately linear trend is observed that spans multiple ballistic coefficient and entry velocity cases. The optimized trajectories result in the larger ballistic coefficient cases having a higher SRP ignition velocity; this is can again be attributed to the higher kinetic energies as the ballistic coefficient is increased. Similarly, there is an overall trend of a smaller FPA at SRP ignition for the higher ballistic coefficient cases. However, the SRP ignition altitude is correlated more with ballistic coefficient than ignition velocity, with the larger ballistic coefficient cases requiring a higher altitude at ignition. Finally, it is interesting to observe in Fig. 6 that, at least for the 450 kg/m2 ballistic coefficient case, the PMF is relatively insensitive to changes in landing site elevation (with higher elevations resulting in a slightly increased PMF).

Figure 7 provides the altitude vs. velocity plots for two SRP trajectories. First, it is interesting to observe that enforcing a 4-*g* limit constraint causes the SRP entry phase to fly higher, and leads to an earlier/higher-altitude SRP ignition. Furthermore, it can be seen that the elimination of a more restrictive parachute deployment Mach-*q* box allows the SRP configurations to fly to much lower altitudes before engine ignition as compared with the MSL parachute deployment conditions. This is expected, as the SRP propulsion remains active until touchdown, and delaying ignition to the latest possible time will reduce the amount of propellant required.

Based on the parametric results, mass sizing was performed to estimate the useful landed payload mass capability of each configuration based on the required PMF and ballistic coefficient. As can be seen in Fig. 8, the larger ballistic coefficient configurations result in a higher landed mass

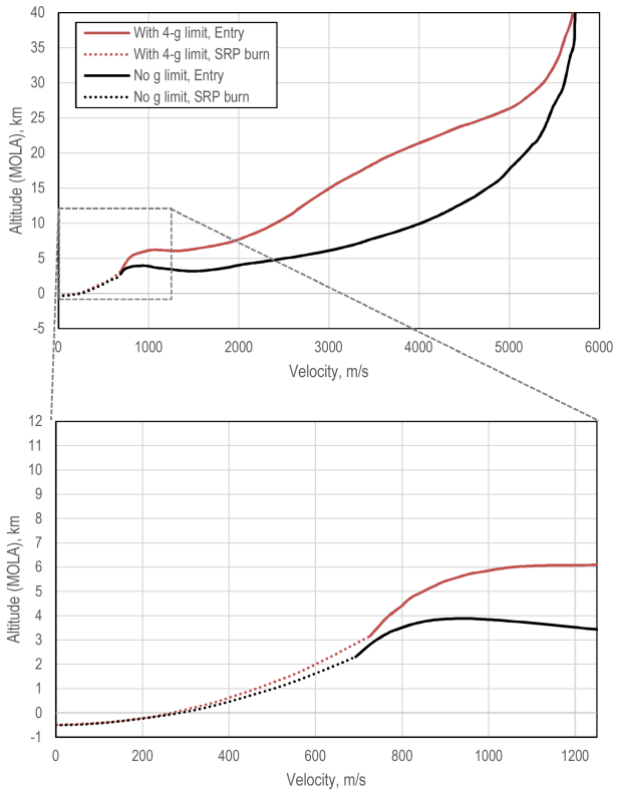

Fig. 7. SRP trajectories with and without 4-*g* limit constraint.

capability (as expected). Similarly, the landed mass in general decreases as the entry velocity (and hence PMF) increases. As reflected in the trajectory PMF results, the *T/W* parameter shows a relatively small impact on landed mass, whereas higher landing site elevations lead to lower landed mass capability. It is interesting to note that while the 4-*g* deceleration constraint had only a small impact on the trajectory PMF results, there is a significant reduction in the useful landed mass. This is primarily due to increased aeroheating loads for the lower-deceleration trajectories, which results in a higher TPS mass fraction (and hence reduction in payload capability). Finally, a comparison of the subsystem mass breakout for the 300 and 450 kg/m2 ballistic coefficient cases is compared with MSL in Fig. 9, and highlights the additional landed mass capabilities of SRP-based configurations vs. the MSL parachute-based architecture.

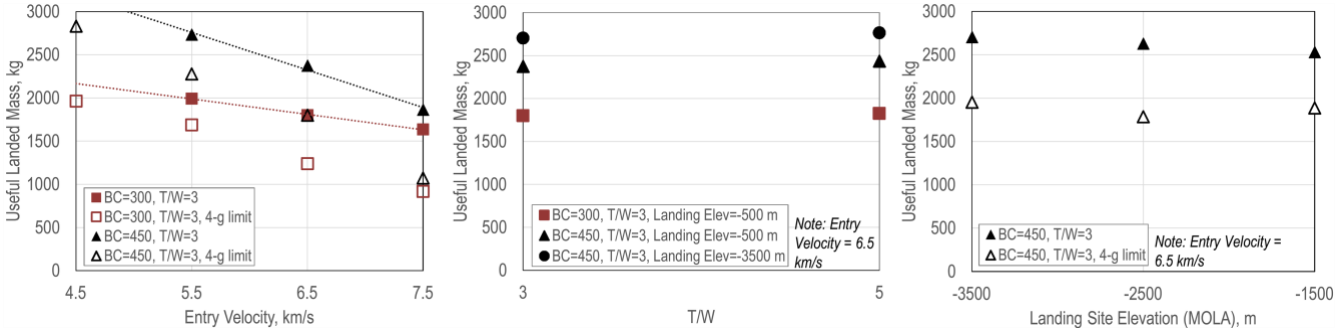

Fig. 8. Mass-sizing results for various SRP design trajectories.

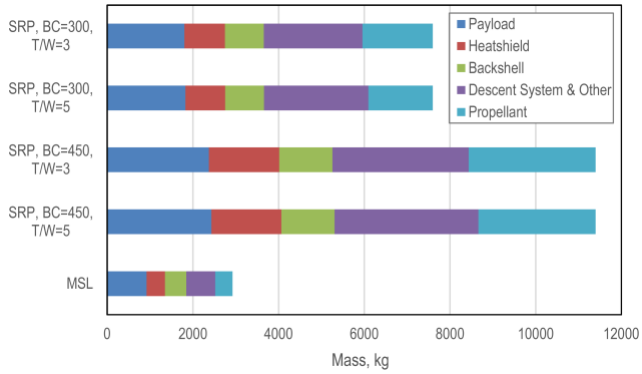

Fig. 9. Mass breakdown for SRP configurations.

5. Conclusion

The present study performed a parametric investigation into the use of Supersonic Retro-Propulsion to enable future high-mass Mars missions. The propellant mass fraction required for SRP was found to be relatively insensitive to Thrust/Weight, landing site elevation, and the application of a 4-*g* deceleration limit. On the other hand, mass-sizing results showed a stronger sensitivity to these parameters based on other aspects of the vehicle design (e.g., TPS mass). Overall, the results indicated that high-ballistic coefficient SRP configurations require propellant mass fractions on the order of 20-25% of the entry mass, yet because of the much larger entry masses compared to MSL, can still land approximately twice the payload mass of MSL using an entry vehicle <5% larger in diameter.

Acknowledgments

©2017 California Institute of Technology. This research was carried out at the Jet Propulsion Laboratory, California Institute of Technology, under a contract with the National Aeronautics and Space Administration. This work was supported by the JPL Mars Formulation Office (6000), and includes contributions from a number of individuals at JPL, including: Joel Benito, Rob Grover, Emily Howard, Ashley Karp, Eddie Lau, Rob Manning, Barry Nakazono, Connor Noyes, Hoppy Price, Dan Scharf, Robert Shotwell, Evgeniy Sklyanskiy, Christine Szalai, and David Vaughan.

References

1) Steltzner, A. D., San Martin, A. M., Rivellini, T. P., Chen, A., and Kipp, D.: Mars Science Laboratory Entry, Descent, and Landing System Development Challenges, *J. Spacecraft and Rockets*, **51** (2014), pp. 994-1003.
2) SpaceX, http://www.spacex.com (accessed October 27, 2016).
3) Lobbia, M. A.: Sizing Methods for Advanced Mars Entry Descent and Landing Systems, 13th International Planetary Probe Workshop (2016).
4) Price, H., Manning, R., Sklyanskiy, E., and Braun, R.: A High-Heritage Blunt-Body Entry, Descent, and Landing Concept for Human Mars Exploration, AIAA Paper 2016-0129, (2016).
5) Squyres, S.: *Visions and Voyages for Planetary Science in the Decade 2013-2022*, National Academies Press (2011).
6) Perino, S., Cooper, D., Rosing, D., Giersch, L., Ousnamer, Z., Jamnejad, V., Spurgers, C., Redmond, M., Lobbia, M., Komarek, T., and Spencer, D.: The Evolution of the Orbiting Sample Container for a Future Mars Sample Return, IEEE Paper AC-2.0621 (2017).
7) Benito, J., Noyes, C., Shotwell, R., Karp, A., Nakazono, B., Singh, G., Schoenenberger, M., Korzun, A., Lobbia, M., and Brandeau, E.: Hybrid Propulsion Mars Ascent Vehicle Concept Flight Performance Analysis, IEEE Paper AC-8.1304 (2017).
8) NASA Launch Services Program Performance Website, https://elvperf.ksc.nasa.gov [accessed 3 March 2017].
9) Prabhu, D. and Saunders, D., "On Heatshield Shapes for Mars Entry Capsules," AIAA Paper 2012-0399 (2012).
10) Benito, J., Sklyanskiy, E., Brandeau, E., and Sell, S., "Powered Descent Guidance Strategy and Algorithms for Mars Landing Using Supersonic Retropropulsion," IEEE Paper AC-2.0306 (2017).
11) Noyes, C., Wolf, A., and Benito, J., "High Ballistic Coefficient Mars EDL With Supersonic Retropropulsion," AAS Paper 17-034 (2017).
12) Lobbia, M. A., "Sizing Methods for Advanced Mars Entry Descent and Landing Systems," 13th International Planetary Probe Workshop (2016).
13) Cutts, J., Arnold, J., Venkatapathy, E., Kolawa, E., Munk, M., Wercinski, P., Laub, B., "Technology for Entry Probes," 2nd International Planetary Probe Workshop (2004).
14) Korzun, A., Cruz, J., and Braun, R., "A Survey of Supersonic Retropropulsion for Mars Entry, Descent, and Landing," IEEE Paper AC-2008-1246 (2008).